

Multimodal Nanoprobes for Radionuclide and Five-Color Near-Infrared Optical Lymphatic Imaging

Hisataka Kobayashi,^{†,*} Yoshinori Koyama,[†] Tristan Barrett,[†] Yukihiro Hama,[†] Celeste A. S. Regino,[‡] In Soo Shin,[§] Beom-Su Jang,[§] Nhat Le,[§] Chang H. Paik,[§] Peter L. Choyke,[†] and Yasuteru Urano[⊥]

[†]Molecular Imaging Program and, [‡]Radiation Oncology Branch, Center for Cancer Research, National Cancer Institute, National Institutes of Health, Bethesda, Maryland 20892-1088, [§]Nuclear Medicine Department, Warren Magnuson Clinical Center, National Institutes of Health, Bethesda, Maryland 20892, and [⊥]Graduate School of Pharmaceutical Sciences, The University of Tokyo, 7-3-1 Hongo, Bunkyo-ku, Tokyo 113-0033, Japan

ABSTRACT Current contrast agents generally have one function and can only be imaged in monochrome; therefore, the majority of imaging methods can only impart uniparametric information. A single nanoparticle has the potential to be loaded with multiple payloads. Such multimodality probes have the ability to be imaged by more than one imaging technique, which could compensate for the weakness or even combine the advantages of each individual modality. Furthermore, optical imaging using different optical probes enables us to achieve multicolor *in vivo* imaging, wherein multiple parameters can be read from a single image. To allow differentiation of multiple optical signals *in vivo*, each probe should have a close but different near-infrared emission. To this end, we synthesized nanoprobes with multimodal and multicolor potential, which employed a polyamidoamine dendrimer platform linked to both radionuclides and optical probes, permitting dual-modality scintigraphic and five-color near-infrared optical lymphatic imaging using a multiple-excitation spectrally resolved fluorescence imaging technique.

KEYWORDS: dendrimer · scintigraphy · near-infrared · fluorescence imaging · multiple modalities · multiple colors · lymphatic imaging

No imaging modality is perfect. Each has its own distinct advantages and limitations. The simultaneous use of two or more modalities can help to overcome the limitation of each individual method and increase or improve the information obtained during an examination session. The combined use of computed tomography (CT) and positron emission tomography (PET) is a successful example of multimodal imaging: CT provides high-resolution anatomical detail, and PET provides functional information.¹ Currently they are very few examples of multimodal imaging probes that can be detected by more than one technique: dual agents for recognition by both radionuclide and optical imaging,^{2,3} or magnetic resonance (MR) and optical imaging.^{4–8}

Furthermore, the conventional imaging methods are generally monochrome and only able to detect one contrast agent at a time, limiting us to single parametric data.

Single-photon scintigraphy has been shown to have potential for simultaneously detecting two different imaging agents, *i.e.*, technetium-99m and thallium-201, by energy resolution.⁹ However, in this case, both the spatial and the energy resolutions were poor and did not allow for the reconstruction of a precise image from each agent. Multicolor optical imaging is simple to achieve with the technique of spectrally resolved imaging. Herein, two or more optical agents can be differentiated on the basis of their different emission spectra. Multicolor imaging is already commonplace in microscopic imaging and is beginning to be utilized for *in vivo* imaging.^{10–12} However, *in vivo* imaging is essentially limited to long-wavelength dyes that emit in the near-infrared (NIR) range (650–850 nm), in order to maximize depth penetration and limit the autofluorescence, background signal.¹³

With this in mind, we have synthesized multimodal, multicolor nanosized imaging probes with nearly identical chemical characteristics. This single-injection imaging probe offers the potential for both multimodal imaging and multicolor resolution.

RESULTS AND DISCUSSION

Using a generation-6 PAMAM dendrimer with an ethylenediamine core as the platform component, ¹¹¹In-labeled radionuclide/five-color NIR optical dual-modal imaging probes were successfully synthesized with multiple steps, as shown in Figure 1. The final products contained 120 SCN-Bz-DTPA molecules and four NIR dyes covalently conjugated with the terminal amino groups. All probes were ~8 nm in diameter, as determined by both dynamic

*Address correspondence to kobayash@mail.nih.gov.

Received for review June 11, 2007 and accepted October 26, 2007.

Published online November 30, 2007.
10.1021/nn700062z CCC: \$37.00

© 2007 American Chemical Society

light scattering (DLS, 8.1 ± 0.1 nm) and gel-filtration (8.5 nm) (Figure 2). Both radionuclide imaging and five-color NIR spectral fluorescence imaging were able to show the lymphatic drainage patterns in the head and neck regions of the mice examined (Figure 3a). Visualization of lymphatic drainage was consistently seen even after shuffling the pattern of injection sites (Figure 3c). All draining lymph nodes (LNs) were subsequently validated by both *ex vivo* radionuclide and five-color NIR spectral fluorescence imaging of the resected LNs, and they were confirmed to represent LNs on the cut section (Figure 3b,d). The radionuclide imaging provided semiquantitative information in addition to the qualitative five-color NIR optical imaging both *in vivo* and *ex vivo* that re-evaluated the variation of lymphatic drainage even in mice of the same strain.^{11,14}

The design of the final product, G6-(Bz-DTPA)₁₁₉-(NIR)₄-(Bz-DTPA-¹¹¹In)₁ (**c**), was rationally designed on the basis of the need to develop a successful and easy-to-use dual-modal multicolor lymph node imaging agent. Bz-DTPA molecules were conjugated to more than half of the available surface amine residues on a dendrimer molecule for the following reasons: (1) suppressing the polycation toxicity of dendrimer by changing the charge,¹⁵ (2) facilitating efficient and stable ¹¹¹In labeling to eventually enable this agent to be produced in a kit form by adding a sufficient number of chelate molecules, (3) leaving open the possibility to conjugate another metal for additional imaging applications (e.g., Gd ions for MRI contrast),^{8,16} and (4) retaining terminal amino groups for conjugation to targeting ligands.¹⁷ The kit form for labeling the dendrimer with ¹¹¹In would require no purification with gel filtration after mixing with ¹¹¹In acetate and, thus, facilitates use in clinical practice. In reality, ITLC data showed that >96.9% of ¹¹¹In was associated with final product **c** in all five compounds before purification, indicating high coefficients of binding (Supporting Information, Figure 1a). The additional purification step using G-50 columns did not show any advantages over the use of prepurified compounds (Supporting Information, Figure 1b). Therefore, as we intended, intermediate product **b** could be radiolabeled with ¹¹¹In acetate just by mixing, and this enables the use of **b** as a prelabeling kit form.

Four NIR dye molecules were conjugated with a single molecule of intermediate product **a**. Since the quantum yield of each NIR dye molecule generally decreased when more than two dyes were conjugated with a G6 dendrimer-DTPA conjugate,⁸ the quantum yield of a conjugate did not increase proportionally as the number of conjugated dyes increased. In addition, if too many dyes were placed on a single G6 conjugate, the dyes

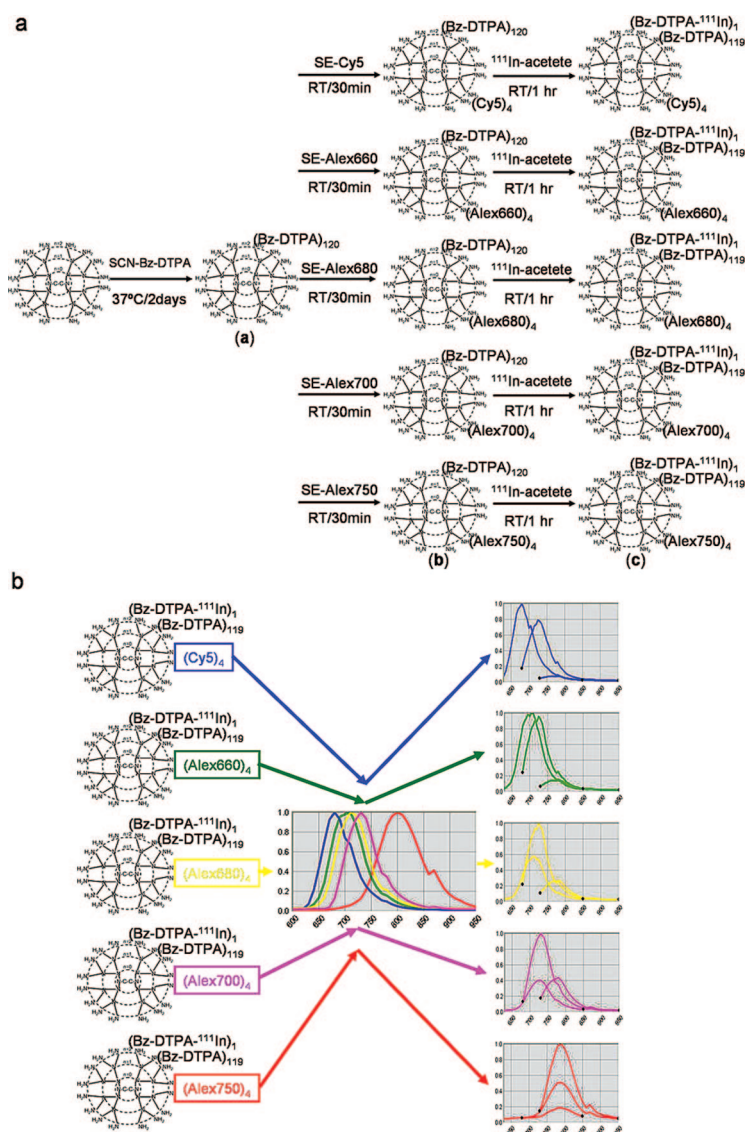


Figure 1. Schema of the synthesis method and the spectral library of nanoprobe. The brief synthesis method and single and multiple emission spectra of each nanoprobe are schematically shown. As for multiple emission spectra, curves 1, 2, and 3 in each spectrum were obtained with three different combined excitation/emission filter settings: 575–605 nm/630–850 nm, 615–665 nm/680–950 nm, and 671–705 nm/730–950 nm, respectively.

quenched.^{8,18} Therefore, four NIR dye molecules on each dendrimer conjugate was proved to be the optimal design.

Local lymphatic drainage is an important route for the metastasis of cancer cells. To this end, identification of the sentinel lymph node and its biopsy has recently become a common staging procedure for cancers which frequently metastasize to the local lymph nodes, *i.e.*, breast cancer^{19,20} and malignant melanoma.^{21,22} However, access to the lymphatic vessels is difficult.²³ Unlike the blood circulation, the lymphatics are one-way, single circulatory systems, from peripheral to central. Furthermore, the lymphatic vessels are complicated small structures, making direct cannulation difficult.²⁴ Thus, indirect uptake following

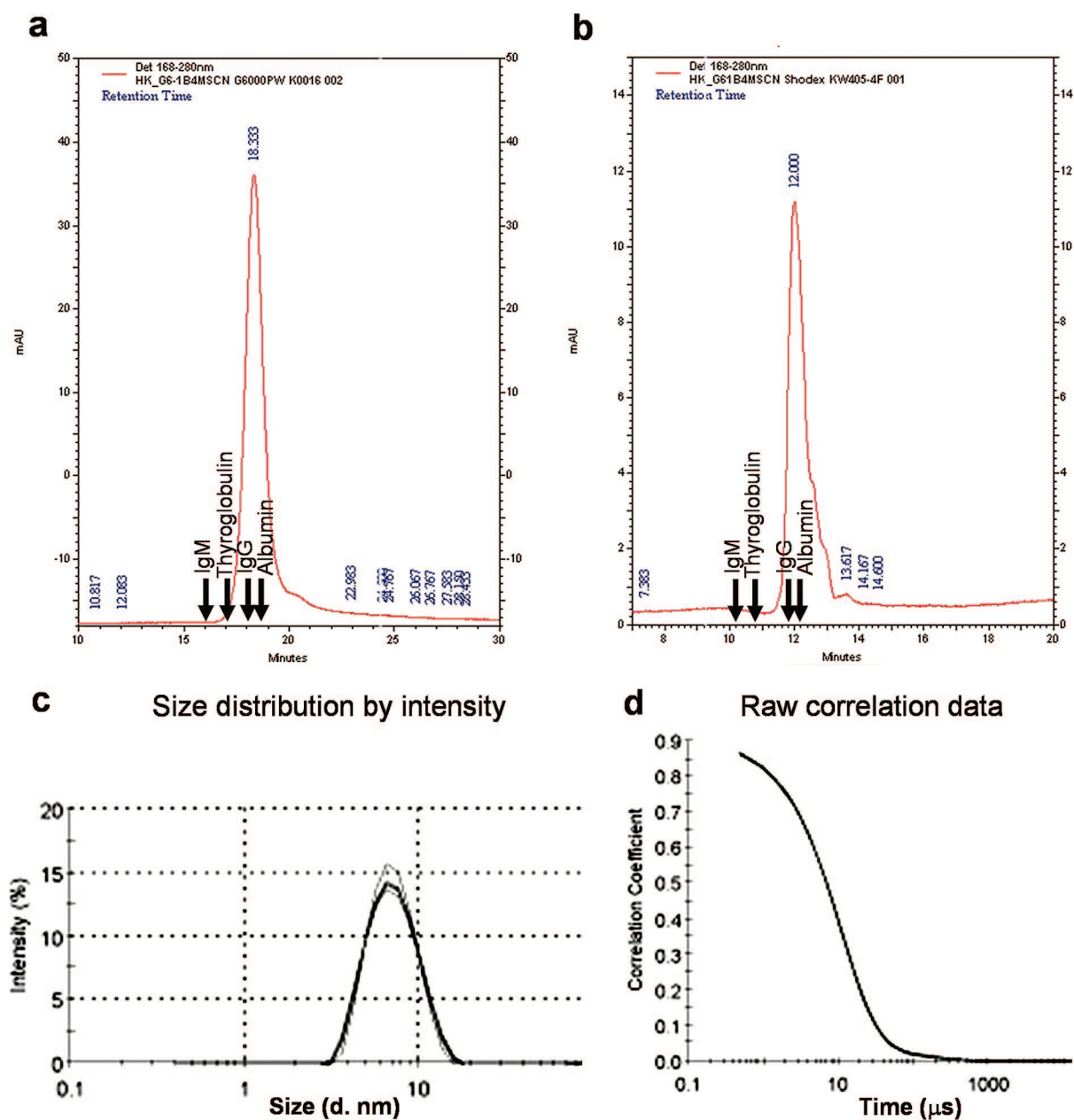


Figure 2. Size measurements. HPLC traces of G6-(Bz-DTPA)₁₂₀ using TSK G6000PW (a) and Shodex KW405-4F (b) are shown. Standard proteins: IgM (24 nm), 16.08 and 10.10 min; thyroglobulin (17 nm), 17.12 and 10.78 min; IgG (11 nm), 18.17 and 11.85 min; and bovine albumin (7 nm), 18.42 and 12.09 min. The calculated diameter with gel filtration using both columns was 8.5 nm. DLS traces of five runs for G6-(Bz-DTPA)₁₂₀ were identical in terms of both distribution of molecular size (c) and correlation coefficient (d). Two other probes (G6-(Bz-DTPA)₁₂₃ and G6-(Bz-DTPA)₁₁₃), which were not used for the synthesis of the final product, demonstrated identical DLS traces ($n = 5$) and size distributions in each sample, as shown in panels c) and d). The calculated diameter with DLS was 8.1 ± 0.1 nm.

interstitial injection of an agent is preferable, although it brings with it greater concerns regarding the pharmacokinetics of their lymphatic drainage. In order to visualize the local lymphatic drainage and detect sentinel lymph nodes (SLNs), the two most commonly used methods employ peritumoral injections of either a radionuclide-labeled sulfur or albumin colloid or isosulfan blue dye.²⁵ Radionuclide imaging has the advantage of increased depth detection but is limited in its spatial resolution.²⁶ The dye method requires dissection of tissue until the “dyed” SLN is visually detected. In addition, staining of the blue dye at the injection site

may present a potent cosmetic problem for breast cancer patients, who subsequently receive breast-conserving surgery. NIR optical imaging offers a means to overcome some of these limitations, because the imaging agents are colorless and can be detected through tissue for 1–2 cm. Indeed, NIR fluorescent quantum dots (QDs) have been employed successfully for *in vivo* imaging of the lymphatics in order to detect the SLN arising from breast tissue.²⁷

However, optical imaging using QDs is still limited in its depth of penetration and by the potential toxicity of the probes, which contain heavy metals, *e.g.*, cad-

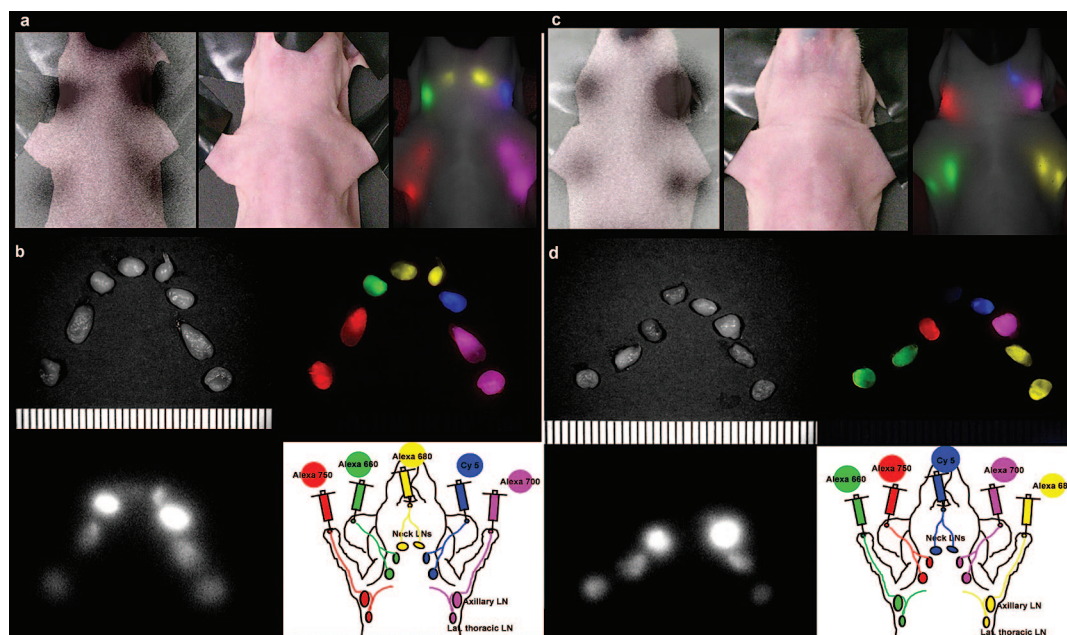


Figure 3. *In vivo* dual-modal, five-color lymphatic drainage imaging with the ability to visualize five distinct lymphatic drainages. (a) *In vivo* multiexcitation spectral fluorescence (right) and *post mortem in situ* radionuclide (left) images of a mouse injected with five distinct G6-(Bz-DTPA)₁₁₉-(NIR)₄-(Bz-DTPA-¹¹¹In)₁ nanoprobe intracutaneously into the middle digits of the bilateral upper extremities, the bilateral ears, and at the median chin, as shown in the schema (mouse 7 in Table 1). Five primary draining lymph nodes were simultaneously visualized with different colors through the skin in the *in vivo* spectral fluorescence image and are more quantitatively seen in the radionuclide image. (b) *Ex vivo* spectral fluorescence and radionuclide images of resected eight draining lymph nodes correlate well to the *in vivo* imaging. (c,d) Images of a different mouse (mouse 8 in Table 1), given shuffled injections. The imaging results were consistent for all mice examined.

mium and selenium in QDs.^{28,29} In addition, in order to make multicolor QDs, each QD must be a slightly different size (~2 nm), which might lead to changes in the kinetics of their lymphatic drainage, especially from subcutaneous tissue such as the breast, where the lymphatic drainage is not as active as in intradermal tissue.¹¹ In order to overcome the limitation of depth, we have recently reported an MRI and NIR optical dual-modal dendrimer-based probe for SLN detection. However, the low sensitivity of MRI for gadolinium contained in the dendrimer structure necessitates a relatively large dose of the agent,⁸ and MRI is relatively impractical for imaging prior to surgery.

In order to minimize these problems, we have developed a series of dual-modal imaging probes with similar chemical and physical characteristics, containing both radionuclide and multicolor organic NIR fluorophores based on a dendrimer platform. Radionuclide imaging of this dual-modal imaging probe allows increased depth penetration and absolute quantification, whereas multicolor NIR optical imaging offers excellent real-time spatial resolution and the ability to distinguish multiple lymphatic drainages. Both of these methods have a matched high sensitivity that allows for minimization of the required injection dose.

Using QDs, it is possible to obtain five separate emissions within the NIR range from five distinct organic NIR dyes with sufficient signal strength, using a single excitation light. Unfortunately, QDs are unlikely to be

used in humans as currently constituted. It was difficult to resolve the spectra of the five distinct organic NIR dyes using a single-excitation light source because of either low excitation/sensitivity for one or more NIR dyes or cross-contamination of two NIR dyes (Supporting Information, Figure 2). Therefore, we employed three different excitation filters to differentially excite five distinct organic NIR dyes in the 650–800 nm range (Figure 1). The use of organic NIR dyes enabled us to conjugate five different NIR fluorophores to PAMAM dendrimers with nearly identical size and chemical characteristics. Chelating a radionuclide to the dendrimer was also stably performed because a large number of chelating agents were conjugated on the surface of the dendrimer. Therefore, each injection was performed with a nearly identical construct with similar bright emission light, differing only in the wavelength of the NIR light emitted, so that successful images could be taken even after shuffling the patterns of injection.

In conclusion, multimodal, multicolor nanosized imaging probes for radionuclide and NIR fluorescence imaging were successfully synthesized and applied for *in vivo* lymphatic imaging of the head and neck region of mice. Radionuclide imaging provided semiquantitative information, while optical imaging provided qualitative information for each of the five lymphatic basins, with excellent spatial resolution. This method may find application in sentinel node imaging of human tumors.

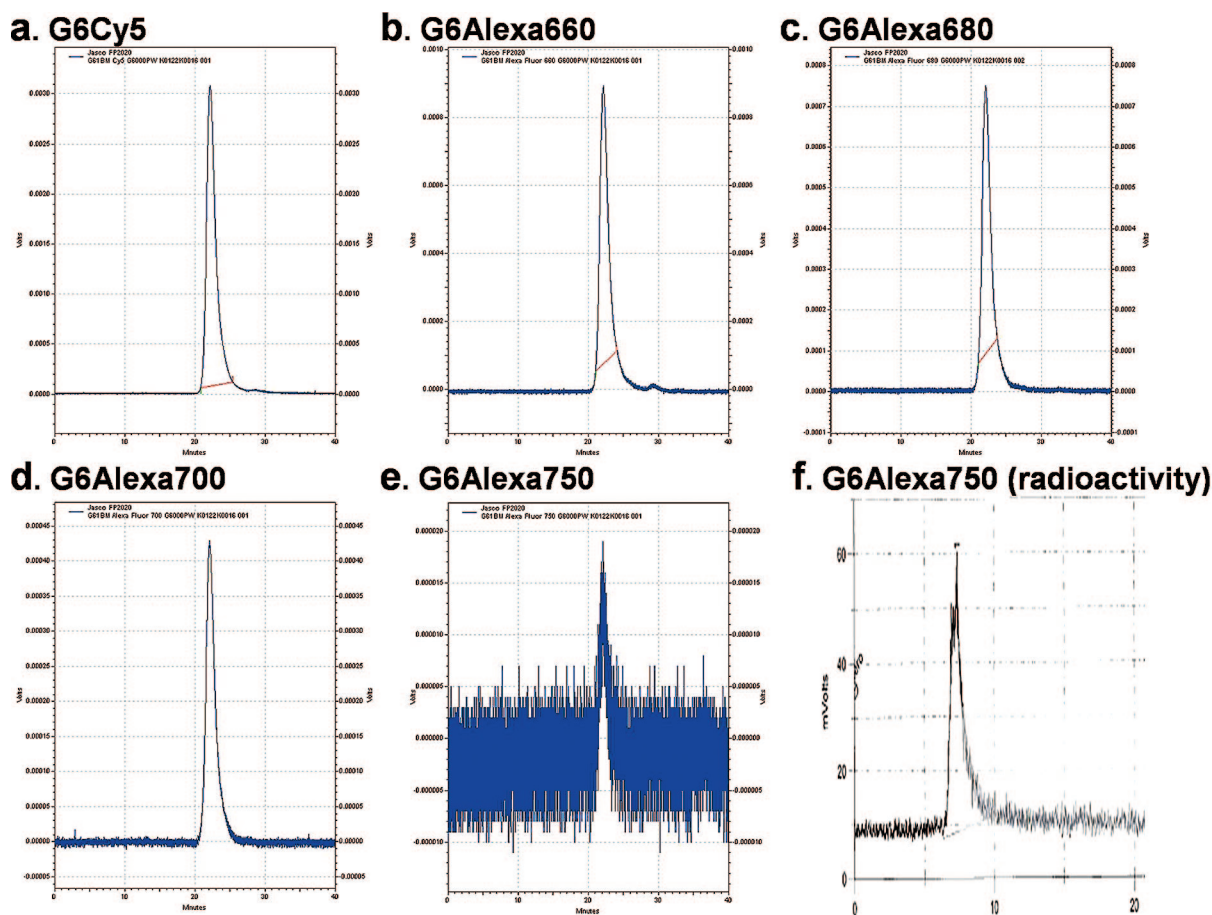


Figure 4. Fluorescent and radioactive purity of the final compound **c** was >98%. HPLC traces of all five final products **c**: G6-(Bz-DTPA)₁₁₉-(NIR)₄-(Bz-DTPA-¹¹¹In)₁ (NIR dyes: **a**, Cy5; **b**, Alexa660; **c**, Alexa680; **d**, Alexa700; **e**, Alexa750) obtained with a fluorescence detector are shown. Peak retention times of all five compounds are 20.67 min on the size-exclusion HPLC using a TSK G6000PW column. Since the fluorescence detector was less sensitive for Alexa750, resulting in small peaks, another HPLC trace of G6-(Bz-DTPA)₁₁₉-(Alexa750)₄-(Bz-DTPA-¹¹¹In), obtained with a radioactivity detector is shown. The peak retention time of this compound is 7.31 min on the size-exclusion HPLC using a TSK G3000PWxL column. The other four compounds showed identical radioactive HPLC traces and exactly the same retention time.

METHODS

Conjugation of the Chelating Agent to Dendrimers. A polyamidoamine dendrimer (PAMAM-G6, Aldrich Chemical Co., Milwaukee, WI) with an ethylenediamine core, the generation-6 interior ($G = 6$), maximum 256 terminal primary amino groups, and a molecular weight of 58 048 Da was used for the basic platform structure. The scheme of the synthetic reaction is shown in Figure 1. PAMAM-G6 solution concentrated to 12 mg (210 nmol) in 2 mL of phosphate buffer at pH 8.5 was reacted with 60 mg (~85 μ mol) of 2-(*p*-isothiocyanatobenzyl)diethylenetriaminopentaacetic acid (SCN-Bz-DTPA, ~700 Da, Macrocyclics, Dallas, TX) at 37 °C for 48 h. The resulting preparation was purified by diafiltration using a Centricon 30 instrument (Amicon Co., Beverly, MA). The number of SCN-Bz-DTPA molecules conjugated per dendrimer was determined by a previously described ¹¹¹In-labeling assay.^{30,31} Briefly, a 5 μ L aliquot of the reaction mixture was reacted with ¹¹¹In chloride in 45 μ L of 0.2 M sodium acetate buffer at pH 4.2 for 1 h at room temperature. The radiolabeled sample was analyzed with a size-exclusion high-performance liquid chromatograph equipped with a TSK G3000SWxL column (Tosoh Bioscience LLC, Montgomeryville, PA; 0.067 M PB, 0.1 M KCl, pH 6.8; 1 mL/min) and an on-line radioactivity detector (Bioscan, Washington, DC). The HPLC profile showed 29% of the total ¹¹¹In radioactivity was associated with the PAMAM-G6 fraction. Therefore, 120 SCN-Bz-DTPA molecules were conjugated per one PAMAM-G6 molecule (**a**, G6-(Bz-DTPA)₁₂₀ in Figure 1, MW = 120 kD).

Conjugation of Near-Infrared Fluorescent Dyes. Amino-reactive Alexa 660, 680, 700, and 750-succinimidyl ester were purchased from Molecular Probes Inc. (Eugene, OR). Amino-reactive Cy5-succinimidyl ester was purchased from GE Healthcare Limited (Piscataway, NJ). At room temperature, 2.0 mg (17 nmol) of compound **a** in 400 μ L of 0.3 M Na₂HPO₄, pH 8.5, was rapidly mixed with 170 nmol (34 μ L/5 mM) of each of the fluorescent dyes and succinimidyl ester in DMSO, and the reaction mixture was incubated for 30 min. The mixture was purified with Sephadex G25 (PD-10, GE Healthcare, Milwaukee, WI).

The G6-(Bz-DTPA)₁₂₀ concentration of NIR dye-conjugated samples was determined with Coomassie Plus protein assay kit (Pierce Chemical Co., Rockford, IL) by measuring the absorption at 595 nm with a UV-vis spectrometer (8453 Value UV-Vis system, Agilent Technologies, Palo Alto, CA) using known concentrations of G6-(Bz-DTPA)₁₂₀ (20, 50, and 100 μ g/mL) as standard solutions. The concentrations of Cy5 and Alexa660, 680, 700, and 750 were measured by their absorption at 651, 665, 681, 703, and 753 nm, respectively, using the UV-vis system to confirm the number of fluorophore molecules conjugated with each G6 dendrimer molecule. The number of fluorophore molecules per G6-(Bz-DTPA)₁₂₀ was 4.1, 3.9, 3.6, 3.9, and 4.0 for Cy5, Alexa660, 680, 700, and 750, respectively (compound **b**, G6-(Bz-DTPA)₁₂₀-(NIR)₄ in Figure 1). The yields of **b** were 91–93% for G6-(Bz-DTPA)₁₂₀, and 36–41% of NIR dye molecules were conjugated with G6-(Bz-DTPA)₁₂₀.

Radiolabeling with ¹¹¹In. Carrier-free ¹¹¹InCl₃ was purchased from PerkinElmer (Wellesley, MA). Dendrimers conjugated with NIR dyes (G6-(Bz-DTPA)₁₂₀-(NIR)₄) were reacted with ¹¹¹In in 0.2

M sodium acetate buffer at pH 4.2 for 1 h at room temperature, as previously described.³² DTPA solution at a final concentration of 0.2 mM was added to the radiolabeled products to complex potential free ¹¹¹In remaining in the product solution. The specific activities of all radiolabeled nanoprobe were similar, ranging from 12.1 to 12.3 mCi/mg (compound **c**, G6-(Bz-DTPA)₁₁₉⁻(NIR)₄-(Bz-DTPA-¹¹¹In)₁ in Figure 1). The radiolabeling yield of the radiolabeled nanoprobe was >98% as determined by instant thin-layer chromatography (ITLC, Gelman Sciences, Ann Arbor, MI) developed with a solvent mixture containing 3:2:1 methanol/10% ammonium acetate in water/0.5 M citric acid and size-exclusion HPLC using a TSK G3000PWxL column (Tosoh Bioscience LLC, Montgomeryville, PA; 0.067 M PB, 0.1 M KCl, pH 6.8; 1 mL/min). On ITLC, ¹¹¹In-labeled G6 dendrimers remain at the origin, whereas free ¹¹¹In moves to the solvent front as ¹¹¹In-DTPA or ¹¹¹In-acetate.

Retention times of all final products detected by an in-line fluorescence detector (FP2020, Jasco Inc., Easton, MD) were 20.7 min on the size-exclusion HPLC using a TSK G6000PW column (Figure 4a–e), and those detected by an in-line NaI gamma detector (γ RAM, IN/US Systems, Inc., Fairfield, NJ) were 7.3 min on the size-exclusion HPLC using a TSK G3000PWxL column (Figure 4f). Both fluorescent and radioactive purity of all final compounds **c** were >98% on size-exclusion HPLCs.

Measurement of the Physical Size of the Agents. The physical sizes of all agents were analyzed with gel filtration using a HPLC system (System Gold, Beckman Coulter, Inc., Fullerton, CA) equipped with a TSK G6000PW 30 cm column (Tosoh Bioscience LLC, Montgomeryville, PA) and a Shodex KW405-4F 30 cm column (Showa Denko America, Inc., New York, NY) with 0.066 M PBS, and with hydrodynamic light scattering (DLS) using a Malvern Zeta Sizer Nano instrument (Malvern Instruments Ltd., Malvern, UK) with 0.066 M PBS. The size calculation with HPLC was performed by using known-sized pure protein standards: IgM, 22 nm; thyroglobulin, 17 nm; IgG, 11 nm; and albumin, 7 nm. Flow rates were 0.5 mL/min for TSK G6000PW and 0.3 mL/min for Shodex KW405-4F. The absorbance at 280 nm was monitored. DLS was performed using the agent alone before the conjugated NIR dyes (**a**, G6-(Bz-DTPA)₁₂₀ in Figure 1) because NIR fluorescence interfered with the light-scattering signal of DLS.

In Vivo Multiple Excitation Wavelength-Resolved Five-Color Spectral Fluorescence and Radionuclide Imaging. All *in vivo* procedures were carried out in compliance with the Guide for the Care and Use of Laboratory Animal Resources (1996), National Research Council, and approved by the National Cancer Institute Animal Care and Use Committee.

Ten-week-old normal athymic female mice were anesthetized *via* intraperitoneal injection of 1.5 mg/300 μ L sodium pentobarbital (Dainabot, Osaka, Japan). The mice were administered intracutaneous injections of 10 μ L/10 μ Ci (350 pmol for NIR dyes) of each G6-(Bz-DTPA)₁₁₉-(NIR)₄-(Bz-DTPA-¹¹¹In)₁ conjugate into one of five sites: the middle phalange of the left or right upper extremity, the left or right ear, and the median chin. For the first five consecutive mice, only spectral fluorescence imaging was performed. The next five mice only underwent radionuclide imaging. Injection points were rotated in each mouse (as shown in Table 1) in order to validate that changing the injection pattern did not affect the imaging quality. Subsequently, another three consecutive mice received both spectral fluorescence and radionuclide imaging to allow for direct comparison of the imaging techniques.

For spectral fluorescence imaging, within 10 min after injection of the agent, when both lymphatic ducts and lymph nodes could be shown clearly,^{11,33} wavelength-resolved spectral imaging was carried out using a spectral imaging system (Maestro In-Vivo Imaging System, CRi Inc., Woburn, MA). Animals were placed in the supine position while under pentobarbital anesthesia. The injection sites were masked with a nonfluorescent black tape because the signal from the injection site would otherwise overwhelm the dynamic range of the camera, rendering the unmixing algorithm nonfunctional. After obtaining *in vivo* images, lymphadenectomy was performed, and another spectral fluorescence image was obtained during surgery. All of the removed LNs were validated by *ex vivo* spectral fluorescence imaging. Three excitation band-pass and emission long-pass filters of 575–

TABLE 1. Summary of Injection Pattern for *in vivo* Five-Color Spectral Fluorescence Lymphatic Imaging.

animal	injection site				
	right hand	left hand	right ear	left ear	median chin
1	Cy5	Alexa660	Alexa700	Alexa680	Alexa750
2	Alexa680	Alexa700	Alexa750	Cy5	Alexa660
3	Alexa750	Alexa680	Cy5	Alexa660	Alexa700
4	Alexa660	Alexa750	Alexa680	Alexa700	Cy5
5	Alexa700	Cy5	Alexa660	Alexa750	Alexa680
dual-modal					
6	Cy5	Alexa660	Alexa700	Alexa680	Alexa750
7	Alexa750	Alexa700	Alexa660	Cy5	Alexa680
8	Alexa660	Alexa680	Alexa750	Alexa700	Cy5

605/645, 615–665/700, and 671–705/750 nm (excitation/emission) were consecutively used. The tunable filter was automatically stepped in 5-nm increments from 630 to 850, from 680 to 950, and from 730 to 950 nm for 575–605/645, 615–665/700, and 671–705/750 nm filter sets, respectively, using the same exposure time for images captured at each wavelength (Figure 1). Each acquisition with this three-excitation spectral fluorescence imaging technique took approximately 2 min. Collected images were analyzed by the Maestro software (Nuance version 2.22, CRi), which uses multispectral unmixing algorithms to separate autofluorescence from NIR dye signals, and a composite image consisting of all five NIR dye signals and autofluorescence was generated using a spectral library obtained from each lymph node injected with either one of the G6-(Bz-DTPA)₁₁₉-(NIR)₄-(Bz-DTPA-¹¹¹In) solutions.

For radionuclide imaging, within 10 min after injection of the agent, radionuclide imaging was carried out using an imaging plate (BAS-SR 2025, Fujifilm Medical Systems USA, Inc., Stamford, CT). Animals were placed in the supine position on the imaging plate immediately after sacrifice by overdose intravenous injection of pentobarbital. The injection sites of the skin were removed as much as possible because the signal from the injection site would otherwise overwhelm the dynamic range of the imaging plate and contaminate the adjacent background. After obtaining *post mortem in situ* images by 10 min exposure, images were developed with 50 μ m resolution using a high-resolution imaging system (FLA-5100, Fujifilm Medical Systems USA). After obtaining *in vivo* images, lymphadenectomy was performed. All removed LNs were validated using *ex vivo* radionuclide imaging as described above.

For the comparison experiments, *in vivo* multiexcitation spectral fluorescence imaging was performed within 10 min of injection, followed by *post mortem in situ* radionuclide imaging. Spectral fluorescence imaging of *ex vivo* lymph nodes was then carried out, followed by the radionuclide imaging.

Acknowledgment. This research was supported by the Intramural Research Program of the NIH, National Cancer Institute, Center for Cancer Research.

Supporting Information Available: ITLC traces demonstrating no further purification will be needed after mixing G6-(Bz-DTPA)₁₂₀-(NIR)₄ with ¹¹¹In acetate for radiolabeling, and spectral fluorescence images of eight NIR fluorescent dyes to demonstrate that the spectral imaging with any single excitation light source was unable to resolve five NIR dyes. This information is available free of charge *via* the Internet at <http://pubs.acs.org>.

REFERENCES AND NOTES

- Blodgett, T. M.; Meltzer, C. C.; Townsend, D. W. PET/CT: Form and Function. *Radiology* **2007**, *242*, 360–385.
- Bullo, K. E.; Dyszlewski, M.; Prior, J. L.; Pica, C. M.; Sharma, V.; Piwnica-Worms, D. Characterization of Novel Histidine-Tagged Tat-Peptide Complexes Dual-Labeled with (99m)Tc-Tricarboxyl and Fluorescein for Scintigraphy and

- Fluorescence Microscopy. *Bioconjugate Chem.* **2002**, *13*, 1226–1237.
3. Houston, J. P.; Ke, S.; Wang, W.; Li, C.; Sevick-Muraca, E. M. Quality Analysis of *In Vivo* Near-Infrared Fluorescence and Conventional Gamma Images Acquired Using a Dual-Labeled Tumor-Targeting Probe. *J. Biomed. Opt.* **2005**, *10*, 054010.
 4. Huber, M. M.; Staubli, A. B.; Kustedjo, K.; Gray, M. H.; Shih, J.; Fraser, S. E.; Jacobs, R. E.; Meade, T. J. Fluorescently Detectable Magnetic Resonance Imaging Agents. *Bioconjugate Chem.* **1998**, *9*, 242–249.
 5. Josephson, L.; Kircher, M. F.; Mahmood, U.; Tang, Y.; Weissleder, R. Near-Infrared Fluorescent Nanoparticles as Combined MR/Optical Imaging Probes. *Bioconjugate Chem.* **2002**, *13*, 554–560.
 6. Kircher, M. F.; Mahmood, U.; King, R. S.; Weissleder, R.; Josephson, L. A Multimodal Nanoparticle for Preoperative Magnetic Resonance Imaging and Intraoperative Optical Brain Tumor Delineation. *Cancer Res.* **2003**, *63*, 8122–8125.
 7. Dafni, H.; Cohen, B.; Ziv, K.; Israely, T.; Goldshmidt, O.; Nevo, N.; Harmelin, A.; Vlodaysky, I.; Neeman, M. The Role of Heparanase in Lymph Node Metastatic Dissemination: Dynamic Contrast-Enhanced MRI of EB Lymphoma in Mice. *Neoplasia* **2005**, *7*, 224–233.
 8. Talanov, V. S.; Regino, C. A.; Kobayashi, H.; Bernardo, M.; Choyke, P. L.; Brechbiel, M. W. Dendrimer-Based Nanoprobe for Dual Modality Magnetic Resonance and Fluorescence Imaging. *Nano Lett.* **2006**, *6*, 1459–1463.
 9. Foster, G. S.; Bekerman, C.; Blend, M. J.; Byrom, E.; Pinsky, S. M. Preoperative Imaging in Primary Hyperparathyroidism. Role of Thallium-Techetium Subtraction Scintigraphy. *Arch. Otolaryngol. Head. Neck. Surg.* **1989**, *115*, 1197–1202.
 10. Hoffman, R. M. The Multiple Uses of Fluorescent Proteins to Visualize Cancer *In Vivo*. *Nat. Rev. Cancer* **2005**, *5*, 796–806.
 11. Hama, Y.; Koyama, Y.; Urano, Y.; Choyke, P. L.; Kobayashi, H. Simultaneous Two-Color Spectral Fluorescence Lymphangiography with Near Infrared Quantum Dots to Map Two Lymphatic Flows from the Breast and the Upper Extremity. *Breast Cancer Res. Treat.* **2007**, *103*, 23–28.
 12. Kobayashi, H.; Hama, Y.; Koyama, Y.; Barrett, T.; Regino, C. A.; Urano, Y.; Choyke, P. L. Simultaneous Multicolor Imaging of Five Different Lymphatic Basins Using Quantum Dots. *Nano Lett.* **2007**, *7*, 1711–1716.
 13. Mahmood, U. Near Infrared Optical Applications in Molecular Imaging. Earlier, More Accurate Assessment of Disease Presence, Disease Course, and Efficacy of Disease Treatment. *IEEE Eng. Med. Biol. Mag.* **2004**, *23*, 58–66.
 14. Kobayashi, H.; Kawamoto, S.; Sakai, Y.; Choyke, P. L.; Star, R. A.; Brechbiel, M. W.; Sato, N.; Tagaya, Y.; Morris, J. C.; Waldmann, T. A. Lymphatic Drainage Imaging of Breast Cancer in Mice by Micro-Magnetic Resonance Lymphangiography Using a Nano-Size Paramagnetic Contrast Agent. *J. Natl. Cancer Inst.* **2004**, *96*, 703–708.
 15. Kobayashi, H.; Sato, N.; Kawamoto, S.; Saga, T.; Hiraga, A.; Ishimori, T.; Konishi, J.; Togashi, K.; Brechbiel, M. W. 3D MR Angiography of Intratumoral Vasculature Using a Novel Macromolecular MR Contrast Agent. *Magn. Reson. Med.* **2001**, *46*, 579–585.
 16. Kobayashi, H.; Brechbiel, M. W. Nano-Sized MRI Contrast Agents with Dendrimer Cores. *Adv. Drug. Deliv. Rev.* **2005**, *57*, 2271–2286.
 17. Wiener, E. C.; Konda, S.; Shadron, A.; Brechbiel, M.; Gansow, O. Targeting Dendrimer-Chelates to Tumors and Tumor Cells Expressing the High-Affinity Folate Receptor. *Invest. Radiol.* **1997**, *32*, 748–754.
 18. Weissleder, R.; Tung, C. H.; Mahmood, U.; Bogdanov, A., Jr. *In Vivo* Imaging of Tumors with Protease-Activated near-Infrared Fluorescent Probes. *Nat. Biotechnol.* **1999**, *17*, 375–378.
 19. Chao, C.; McMasters, K. M. Sentinel Lymph Node Biopsy in Breast Cancer. *Methods Mol. Med.* **2006**, *120*, 91–111.
 20. Ferrari, A.; Rovera, F.; Dionigi, P.; Limonta, G.; Marelli, M.; Besana Ciani, I.; Bianchi, V.; Vanoli, C.; Dionigi, R. Sentinel Lymph Node Biopsy as the New Standard of Care in the Surgical Treatment for Breast Cancer. *Exp. Rev. Anticancer Ther.* **2006**, *6*, 1503–1515.
 21. Essner, R. Sentinel Lymph Node Biopsy and Melanoma Biology. *Clin. Cancer Res.* **2006**, *12*, 2320s–2325s.
 22. Uren, R. F. Sentinel Lymph Node Biopsy in Melanoma. *J. Nucl. Med.* **2006**, *47*, 191–195.
 23. Moskovic, E.; Fernando, I.; Blake, P.; Parsons, C. Lymphography—Current Role in Oncology. *Br. J. Radiol.* **1991**, *64*, 422–427.
 24. Davis, M. J. An Improved, Computer-Based Method to Automatically Track Internal and External Diameter of Isolated Microvessels. *Microcirculation* **2005**, *12*, 361–372.
 25. Kim, T.; Giuliano, A. E.; Lyman, G. H. Lymphatic Mapping and Sentinel Lymph Node Biopsy in Early-Stage Breast Carcinoma: A Metaanalysis. *Cancer* **2006**, *106*, 4–16.
 26. Alazraki, N. P.; Styblo, T.; Grant, S. F.; Cohen, C.; Larsen, T.; Aarsvold, J. N. Sentinel Node Staging of Early Breast Cancer Using Lymphoscintigraphy and the Intraoperative Gamma-Detecting Probe. *Semin. Nucl. Med.* **2000**, *30*, 56–64.
 27. Kim, S.; Lim, Y. T.; Soltesz, E. G.; De Grand, A. M.; Lee, J.; Nakayama, A.; Parker, J. A.; Mihaljevic, T.; Laurence, R. G.; Dor, D. M.; *et al.* Near-Infrared Fluorescent Type II Quantum Dots for Sentinel Lymph Node Mapping. *Nat. Biotechnol.* **2004**, *22*, 93–97.
 28. Hardman, R. A. Toxicologic Review of Quantum Dots: Toxicity Depends on Physicochemical and Environmental Factors. *Environ. Health Perspect.* **2006**, *114*, 165–172.
 29. Cho, S. J.; Maysinger, D.; Jain, M.; Roder, B.; Hackbarth, S.; Winnik, F. M. Long-Term Exposure to CdTe Quantum Dots Causes Functional Impairments in Live Cells. *Langmuir* **2007**, *23*, 1974–1980.
 30. Kobayashi, H.; Sato, N.; Hiraga, A.; Saga, T.; Nakamoto, Y.; Ueda, H.; Konishi, J.; Togashi, K.; Brechbiel, M. W. 3D-Micro-MR Angiography of Mice Using Macromolecular MR Contrast Agents with Polyamidoamine Dendrimer Core with References to Their Pharmacokinetic Properties. *Magn. Reson. Med.* **2001**, *45*, 454–460.
 31. Kobayashi, H.; Sakahara, H.; Hosono, M.; Shirato, M.; Kondo, S.; Miyatake, S.; Kikuchi, H.; Namba, Y.; Endo, K.; Konishi, J. Scintigraphic Detection of Neural-Cell-Derived Small-Cell Lung Cancer Using Glioma-Specific Antibody. *J. Cancer Res. Clin. Oncol.* **1994**, *120*, 259–262.
 32. Kobayashi, H.; Wu, C.; Yoo, T. M.; Sun, B. F.; Drumm, D.; Pastan, I.; Paik, C. H.; Gansow, O. A.; Carrasquillo, J. A.; Brechbiel, M. W. Evaluation of the *In Vivo* Biodistribution of Yttrium-Labeled Isomers of CHX-DTPA-Conjugated Monoclonal Antibodies. *J. Nucl. Med.* **1998**, *39*, 829–836.
 33. Kobayashi, H.; Kawamoto, S.; Star, R. A.; Waldmann, T. A.; Tagaya, Y.; Brechbiel, M. W. Micro-Magnetic Resonance Lymphangiography in Mice Using a Novel Dendrimer-Based Magnetic Resonance Imaging Contrast Agent. *Cancer Res.* **2003**, *63*, 271–276.